Chem., **26**, 734 (1980).
(17) J. Lankelma and H. Poppe, *J. Chromatogr.*, **149**, 587 (1978).
(18) J. A. Nelson, B. A. Harris, W. J. Decker, and D. Farquhar, *Cancer Res.*, **37**, 3970 (1977).
(19) E. Watson, J. L. Cohen, and K. K. Chan, *Cancer Treat. Rep.*, **62**, 381 (1978).
(20) Y. M. Wang, S. K. Howell, and J. A. Benvenuto, *J. Liq. Chromatogr.*, **3**, 1071 (1980).

ACKNOWLEDGMENTS

Supported by NCI Grant CA-16518-06.

Theoretical and Experimental Studies of Transport of Micelle-Solubilized Solutes

GREGORY E. AMIDON *x, WILLIAM I. HIGUCHI, and NORMAN F. H. HO

Received February 9, 1981, from the *University of Michigan, Ann Arbor, MI 48109.* Accepted for publication April 27, 1981.
*Present address: Pharmacy Research, The Upjohn Company, Kalamazoo, MI 49001.

Abstract □ A physical model describing the simultaneous diffusion of free solute and micelle-solubilized solute across the aqueous boundary layer, coupled with partitioning and diffusion of free solute through a lipoidal membrane, is derived. *In vitro* experiments utilizing progesterone and polysorbate 80 showed excellent agreement between theoretical predictions based on independently determined parameters and experimental results. The physical model predicts that micelles can assist the transport of solubilized solute across the aqueous diffusion layer, resulting in a higher solute concentration at the membrane surface than would be predicted if micelle diffusion is neglected. At high surfactant concentrations, the aqueous diffusion layer resistance can be eliminated and the activity of the solute at the membrane can approach the bulk solute activity. This mechanism could explain observed enhanced absorption rates *in vivo* when both micelle solubilization occurs and the aqueous diffusion layer is an important transport barrier. The importance of determining and defining the thermodynamic activity of the diffusing solute is emphasized.

Keyphrase □ Diffusion—transport of micelle-solubilized solutes, theoretical and experimental □ Solutes—micelle solubilized, transport, theoretical and experimental □ Micelles—theoretical and experimental transport, solutes

The effects of micelle solubilization on the solubility and intestinal absorption of nonpolar solutes are well documented (1–8). Investigations have been performed to delineate the role of surfactants in diffusional transport. As a result of these studies, it is clear that several factors must be considered, such as the thermodynamic activity of the solute, diffusivities of the free solute and micelles, membrane permeability, and the importance of the aqueous diffusion layer in determining the overall transport rate.

BACKGROUND

In a diffusional process (*e.g.*, intestinal absorption), a difference in the thermodynamic activity determines the direction of and driving force for the net transport of mass. Therefore, when micelle solubilization occurs and the thermodynamic activity of solute is lowered, a decreased diffusional rate is expected. On this basis, decreased absorption rates of salicylic acid in the presence of polysorbate 60 from rat intestinal segments were explained (1).

However there are numerous examples of increased absorption rates *in vivo* when solubilizing agents are present (2, 3). For example, the serum blood levels of indoxole when administered in a polysorbate 80 solution to humans were three to four times higher than comparable doses with an aqueous suspension or hard capsule (4). It was shown (5, 6), however, that membrane permeabilities may change in the presence of surfactant, possibly resulting in a net increase in the absorption rate even with a decreased thermodynamic activity of solute in bulk aqueous solution.

Another reason for enhanced absorption in the presence of solubilizing agents is associated with the diffusion of solute in the aqueous phase (*i.e.*, within the aqueous diffusion layer). Westergaard and Dietschy (7) pointed out that, in addition to the importance of bulk solute concentration and membrane permeability in determining absorption rates, the aqueous boundary layer is an important barrier to transport *in vivo* and should be evaluated. They concluded that the apparent functions of the micelle were to overcome the diffusion layer resistance *in vivo* and to deliver a maximum solute concentration to the membrane surface. It was also suggested (8) that the diffusion coefficient of the free solute–micelle complex is important in quantitatively assessing absorption in the presence of micelles.

Thus, it is clear that an evaluation of the aqueous diffusion layer and the physicochemical events occurring within it is necessary in the development of a realistic physical model. Furthermore, micellar diffusion, membrane permeation, and the thermodynamic activity of the solute in the surfactant solution need to be included in any complete analysis. This report presents a comprehensive physical model incorporating all of the principles just discussed. *In vitro* experiments along with independent determinations of all physicochemical parameters defined in the physical model were carried out utilizing progesterone and the nonionic surfactant polysorbate 80. Therefore, theoretical predictions based on independent estimates of the important parameters and experimentally determined fluxes can be compared.

The physical model is defined for two hydrodynamic conditions: the

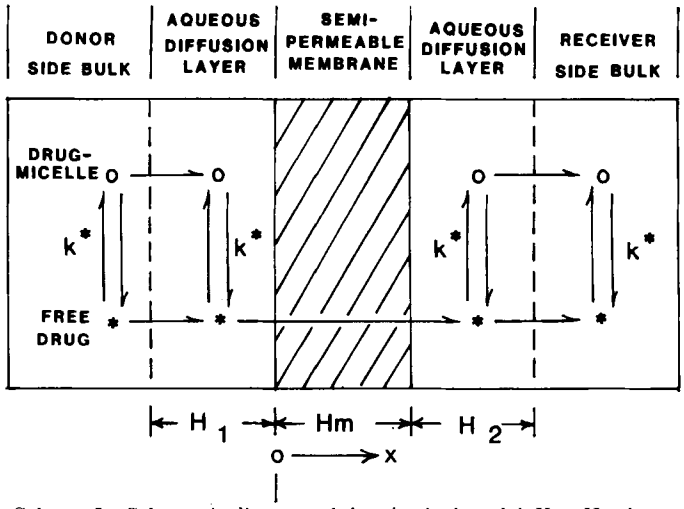

Scheme I—Schematic diagram of the physical model. Key: H_1, *donor side aqueous diffusion layer thickness;* H_m, *semipermeable membrane thickness;* H_2, *receiver side diffusion layer thickness; and* k*, *micelle-free solute equilibrium distribution coefficient.*

[1] Dow Corning, Midland, Mich.

0022-3549/82/0100-0077$01.00/0

stagnant diffusion layer case and the more well-defined hydrodynamic case for the surface of a rotating disk. For this latter situation, the fluid flow within the aqueous diffusion layer is well defined (9) and more easily controlled; it provides insight into actual events occurring within the diffusion layer and places the physical model on a more sound theoretical basis. For hydrodynamic conditions that are not ideal (*i.e.*, many *in vivo* absorption situations), the stagnant diffusion layer approach permits an evaluation of the aqueous diffusion layer resistance to diffusion.

A rotating-membrane diffusion cell similar to that used by Albery *et al.* (10) was employed for the present *in vitro* diffusion experiments. Proper design provides for well-defined hydrodynamics on each side of the rotating semipermeable membrane. Dimethicone (dimethylpolysiloxane[1]) membranes were utilized since they have been shown to maintain their integrity in the presence of surfactants (11) and buffers (12) and are quite permeable to the solutes investigated.

THEORY

Description of Model—The physical model involving the simultaneous diffusion of both free solute and solute solubilized in micelles is shown in Scheme I. Two aqueous compartments are separated by a semipermeable, lipid-like membrane, which permits only the passage of free solute. The donor compartment contains free solute, surfactant, and solute solubilized by the surfactant. It is assumed that the receiver compartment is at an equivalent surfactant concentration. This assumption is not necessary but simplifies the mathematics.

Furthermore, equilibrium between free solute and that solute solubilized in the micelle is assumed to occur at each point in the aqueous phase and in the diffusion layer. This equilibrium distribution coefficient is denoted by k^*; for the present model, it is assumed to be a constant.

The bulk of each aqueous phase is assumed to be well mixed by convection and, therefore, of uniform concentration in each compartment. Adjacent to the membrane is a region of relatively stagnant solution. It is primarily within this region (the aqueous diffusion layer) that concentration gradients of species may exist between the well-stirred bulk and the membrane surface. Under ideal hydrodynamic conditions, such as those of a rotating disk[2], the fluid flow near the surface can be mathematically described and an explicit relationship for the effective diffusion layer thickness can be obtained (13). When hydrodynamic conditions are not well defined, a stagnant diffusion layer model can be used.

Both free solute and micelles that may contain solubilized solute are assumed to diffuse independently across the aqueous diffusion layer. However, only free solute is assumed to partition into and diffuse through the membrane. Therefore, the components of the micelle are conserved in each compartment so that the surfactant concentration is assumed to be constant throughout each bulk phase and the diffusion layers.

Stagnant Diffusion Layer Model—When the aqueous diffusion layer is assumed to be a stagnant solvent layer, the steady-state flux equation for each diffusion layer ($i = 1, 2$) can be written as the sum of the flux of the micelle-solubilized solute and the free solute:

$$J_1 = \frac{D_1^*}{H_1}(C_{b1}^* - C_{s1}^*) + \frac{D_1'}{H_1}(C_{b1}' - C_{s1}') \qquad \text{(Eq. 1)}$$

$$J_2 = \frac{D_2^*}{H_2}(C_{s2}^* - C_{b2}^*) + \frac{D_2'}{H_2}(C_{s2}' - C_{b2}') \qquad \text{(Eq. 2)}$$

where J is the steady-state flux; D is diffusivity; H is effective diffusion layer thickness; C is concentration; the asterisk and prime superscripts denote the micelle-solubilized species and the free solute, respectively; and the subscripts b and s denote the bulk and membrane surface for the donor, 1, and receiver, 2, sides.

The following free solute–micelle-solubilized solute equilibrium is assumed to hold above the critical micelle concentration (CMC) of the surfactant:

$$k^* = \frac{C_i^*}{C_i'(SAA)} \qquad \text{(Eq. 3)}$$

where k^* is the equilibrium distribution coefficient, C_i^* and C_i' are the micelle-solubilized solute concentration and free solute concentration per liter of solution, and (SAA) is the surfactant concentration[3]. This relationship permits the free solute concentration (thermodynamic activity) to be calculated when micelles are present.

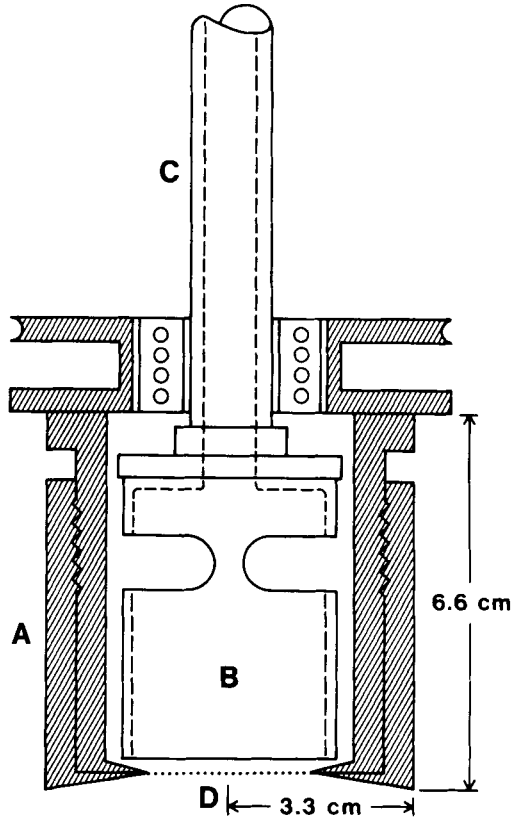

Figure 1—*Schematic diagram of rotating-membrane diffusion cell. Key: A, outer stainless steel cylinder; B, stationary cylindrical baffle; C, sampling port; and D, semipermeable membrane.*

The total bulk and surface concentration for each aqueous compartment can be written:

$$C_{bi} = C_{bi}^* + C_{bi}' = C_{bi}'[1 + k^*(SAA)] \qquad \text{(Eq. 4)}$$

$$C_{si} = C_{si}^* + C_{si}' = C_{si}'(1 + k^*(SAA)] \qquad \text{(Eq. 5)}$$

Eqs. 1 and 2 can be rewritten:

$$J_1 = P_1(C_{b1} - C_{s1}) \qquad \text{(Eq. 6)}$$

$$J_2 = P_2(C_{s2} - C_{b2}) \qquad \text{(Eq. 7)}$$

where P is permeability and:

$$P_i = \frac{D_{\text{eff}}}{H_i} \qquad \text{(Eq. 8)}$$

The effective diffusion coefficient, D_{eff}, is defined as:

$$D_{\text{eff}} = \frac{D_i' + k^*(SAA)D_i^*}{[1 + k^*(SAA)]} \qquad \text{(Eq. 9}a\text{)}$$

An identical way of expressing the effective diffusion coefficient is:

$$D_{\text{eff}} = f'D' + f^*D^* \qquad \text{(Eq. 9}b\text{)}$$

where f' and f^* are the fractions of the total solute in the free form and solubilized form, respectively.

It is evident from Eq. 9*b* that the diffusivity of each aqueous diffusion layer becomes essentially the diffusivity for the micelle-solubilized solute, D^*, when the surfactant concentration is large. At premicellar concentrations and low micellar concentrations, the diffusivity is essentially the diffusivity for free solute, D'.

The steady-state flux of solute through the semipermeable membrane (J_m) can be written as:

$$J_m = \frac{D_m}{H_m}(C_{m1}' - C_{m2}') \qquad \text{(Eq. 10)}$$

where C_{m1}' and C_{m2}' are the free solute concentrations in the membrane at each interface and D_m is the solute diffusivity in the membrane of thickness H_m.

[2] Other geometries such as flow across a flat surface or laminar flow down a tube provide equally well-defined hydrodynamics.

[3] Here (SAA) is equivalent to the concentration of micelles in solution. Therefore, $(SAA) = (SAA)_T - \text{CMC}$, where $(SAA)_T$ is the total surfactant concentration. For surfactants with low CMC values (such as polysorbate 80, CMC $\simeq$ 0.006%): $(SAA) \simeq (SAA)_T$.

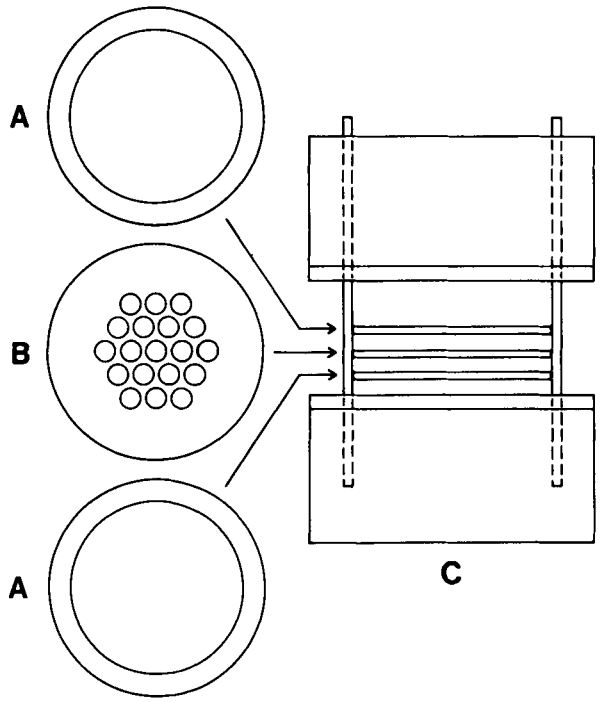

Figure 2—*Membrane support and spacers (each 50-μm thick).*

The membrane–aqueous phase partition coefficient, K, is:

$$K = \frac{C'_{mi}}{C'_{si}} \qquad \text{(Eq. 11)}$$

Combining Eqs. 10 and 11 gives:

$$J_m = \frac{KD_m}{H_m}(C'_{s1} - C'_{s2}) \qquad \text{(Eq. 12)}$$

When the surfactant concentration is the same on each side,[4] the membrane flux can be written in terms of the total solute concentration:

$$J_m = P_m(C_{s1} - C_{s2}) \qquad \text{(Eq. 13)}$$

where:

$$P_m = \frac{KD_m}{H_m[1 + k^*(SAA)]} \qquad \text{(Eq. 14)}$$

The membrane permeability is a function of the surfactant concentration since it is related to the free solute concentration at the membrane surface.

At steady state, the flux of solute through each region must be equal; therefore:

$$J_1 = J_m = J_2 \qquad \text{(Eq. 15)}$$

and:

$$J = P_{\text{eff}}(C_{b1} - C_{b2}) \qquad \text{(Eq. 16)}$$

where the effective permeability coefficient, P_{eff}, is:

$$P_{\text{eff}} = \frac{1}{\frac{1}{P_1} + \frac{1}{P_m} + \frac{1}{P_2}} \qquad \text{(Eq. 17)}$$

The total solute concentration at each interface is given by:

$$C_{s1} = \frac{\left(\frac{1}{P_m} + \frac{1}{P_2}\right)C_{b1} + \left(\frac{1}{P_1}\right)C_{b2}}{\frac{1}{P_1} + \frac{1}{P_m} + \frac{1}{P_2}} \qquad \text{(Eq. 18)}$$

[4] This assumption is not necessary but simplifies the mathematics that follow.

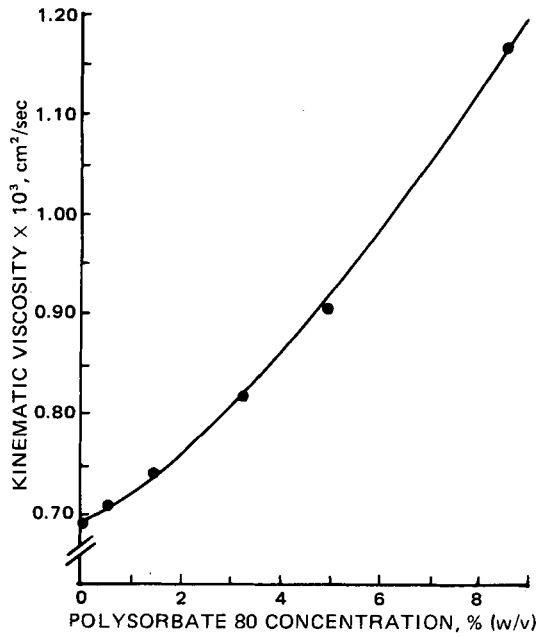

Figure 3—*Kinematic viscosity of polysorbate 80 solutions at 37°.*

$$C_{s2} = \frac{\left(\frac{1}{P_2}\right)C_{b1} + \left(\frac{1}{P_1} + \frac{1}{P_m}\right)C_{b2}}{\frac{1}{P_1} + \frac{1}{P_m} + \frac{1}{P_2}} \qquad \text{(Eq. 19)}$$

Convective Diffusion Layer Model—For the ideal hydrodynamics near the surface of a rotating disk, the convective diffusion equation for mass transfer can be solved (13). The solution predicts solvent movement even immediately adjacent to the rotating surface. Therefore, instead of a stagnant diffusion layer, a dynamic convective diffusion layer is more appropriate. Within this layer (normally ≤50 μm) and extending out into the bulk, there is a gradual transition from an essentially diffusional process at the disk surface to one in which the major transport mechanism is convection.

Under these rotating-disk conditions, the effective diffusion layer thickness is:

$$H = 1.61\nu^{1/6}D^{1/3}\omega^{-1/2} \qquad \text{(Eq. 20)}$$

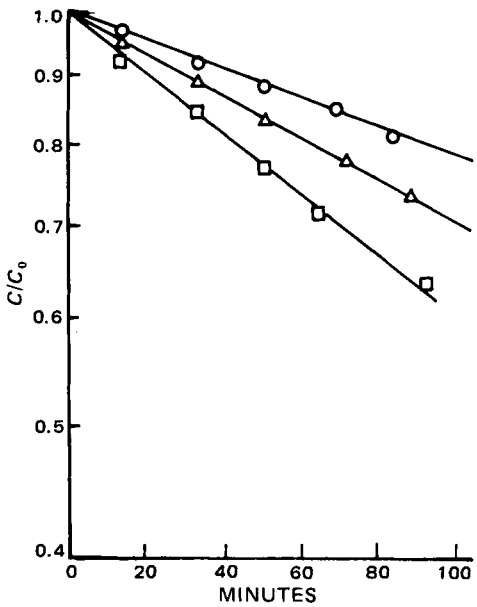

Figure 4—*Semilogarithmic plot of the fraction of radiolabeled capric acid remaining in the donor phase with time when both the donor and receiver side diffusion layers are important. Key:* ○, *60 rpm;* △, *120 rpm; and* □, *300 rpm.*

Table I—Effective Diffusion Coefficients of Progesterone–Polysorbate 80 Solutions

Polysorbate 80 Concentration, % (w/v)	$D_{eff} \times 10^6$, cm^2/sec Trace Concentrations	$D_{eff} \times 10^6$ cm^2/sec Saturated Solutions	$D^* \times 10^6$, cm^2/sec Estimated
0.0	8.50	—	—
0.103	—	6.52	4.68
0.116	6.22	—	4.35
0.514	3.58	—	2.67
0.56	—	2.51	1.49
0.942	3.22	—	2.69
1.96	2.13	—	1.82
2.03	—	1.76	1.46
5.04	1.56	—	1.43

and the steady-state mass flux of solute, J, through the convective diffusion layer can be written:

$$J = \frac{D\,\Delta C}{H} = 0.62D^{2/3}\nu^{-1/6}\omega^{1/2}(C_b - C_s) \qquad \text{(Eq. 21)}$$

where D is the aqueous diffusion coefficient, ν is the kinematic viscosity, and ω is the disk rotation speed in radians per second.

For the simultaneous convective diffusion of free solute and micelle-solubilized solute, Eq. 21 can be modified to:

$$J = 0.62D_{eff}^{2/3}\nu^{-1/6}\omega^{1/2}(C_b - C_s) \qquad \text{(Eq. 22)}$$

where the effective diffusion coefficient, D_{eff}, is defined in Eq. 9*a*.

When the flux of solute through the convective diffusion layer on each side of the semipermeable membrane is given by Eq. 22 and the membrane permeability coefficient is given by Eq. 13, the following equation predicts the total flux of solute (J):

$$J = P_{eff}(C_{b1} - C_{b2}) \qquad \text{(Eq. 23)}$$

where:

$$P_{eff} = \frac{1}{\frac{1}{P_1^c} + \frac{1}{P_m} + \frac{1}{P_2^c}} \qquad \text{(Eq. 24)}$$

and the permeability of each convective diffusion layer, P_i^c, is:

$$P_i^c = \frac{D_{eff}}{H_i} = 0.62D_{eff}^{2/3}\nu^{-1/6}\omega^{1/2} \qquad \text{(Eq. 25)}$$

Both D_{eff} and ν may be functions of surfactant concentration. For simplicity, it is assumed here, as it was in the stagnant diffusion layer model, that the surfactant concentrations in both the donor and receiver sides are equal.

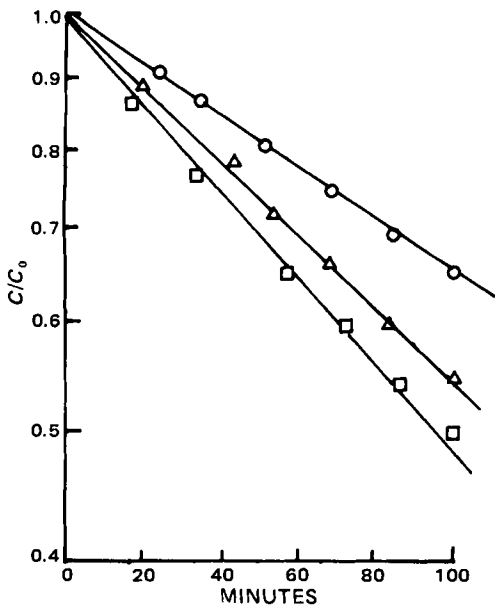

Figure 5—*Semilogarithmic plot of the fraction of radiolabeled capric acid remaining in the donor phase when the receiver side diffusion layer resistance is eliminated by adjustment of pH. Key: ○, 60 rpm; △, 120 rpm; and □, 300 rpm.*

Table II—Reproducibility of Effective Permeability Coefficient Determinations

	Rotation Speed, radians/sec		
	6.28 (60 rpm)	12.57 (120 rpm)	31.42 (300 rpm)
n	5	8	5
$P_{eff} \times 10^4$	6.58	9.77	13.67
$SD \times 10^4$	0.370	0.589	0.733
CV, %	5.6	6.0	5.4

Equation 24 can be rewritten as:

$$\frac{1}{P_{eff}} = \frac{1}{P_1^c} + \frac{1}{P_m} + \frac{1}{P_2^c} \qquad \text{(Eq. 26)}$$

and, using Eq. 25, the following can be derived:

$$\frac{1}{P_{eff}} = 2\left[\frac{\nu^{1/6}}{0.62D_{eff}^{2/3}}\right]\omega^{-1/2} + \frac{1}{P_m} \qquad \text{(Eq. 27)}$$

If one diffusion layer is eliminated, then Eq. 27 reduces to:

$$\frac{1}{P_{eff}} = \left[\frac{\nu^{1/6}}{0.62D_{eff}^{2/3}}\right]\omega^{-1/2} + \frac{1}{P_m} \qquad \text{(Eq. 28)}$$

Thus, Eqs. 27 and 28 offer a convenient way of testing the validity of Eq. 20 for the diffusion layer thickness on each side of the semipermeable membrane.

Diffusion Cell and Membrane Preparation—A diagram of the rotating-membrane diffusion cell is shown in Fig. 1. An outer stainless steel cylinder is connected to a variable-speed motor by a pulley and belt system. In this way, the outer cylinder can be rotated at a variety of speeds with ease. A stationary cylindrical baffle attached to the hollow sampling port is suspended inside the outer cylinder. To allow proper fluid flow inside the cell, two grooves ~1-cm wide are cut 3 cm from the bottom of the inner baffle, which is open.

The outer cylinder can be further disassembled by unscrewing to allow the membrane to be positioned at the bottom of the cell and screwed tightly into place. In addition, at each edge of the membrane, the cylinder is beveled at an angle of ~10° so that fluid flow at the edge is not dis-

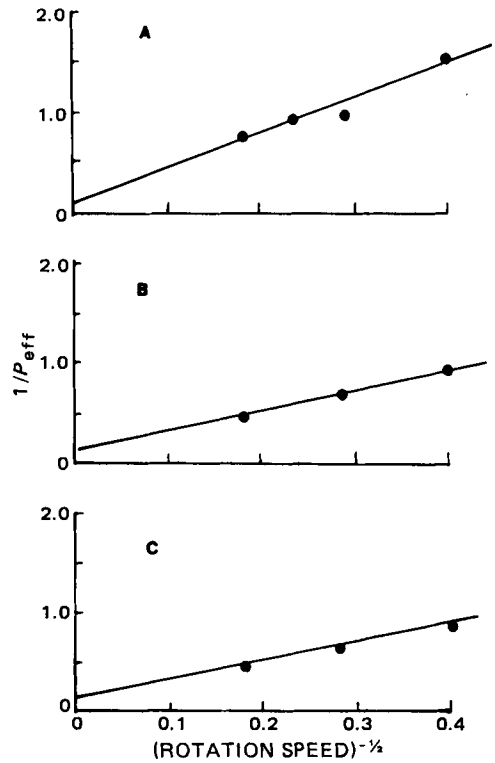

Figure 6—*Permeability coefficient dependence on rotation speed when both donor and receiver side diffusion layer resistances are important (A), outer diffusion layer resistance is eliminated (B), and inner diffusion layer resistance is eliminated (C).*

turbed (10). The cell is immersed in an outer solution of 450 ml, while the inner volume is 70 ml.

Dimethicone, a two-component room temperature vulcanizing dimethyl polysiloxane rubbber, was used as the model membrane. This material forms a nonpolar continuum and is lipid-like in nature, so partitioning and membrane diffusion rather than pore permeation occurs. Unlike more conventional lipid-impregnated membrane filters, it has been shown to be impermeable to ions and buffers and is unaffected by surfactants. These properties, along with the relatively simple procedure for preparing these membranes in the laboratory, indicated it would be a good candidate for model studies.

The membranes were prepared by mixing the catalyst with elastomer base and applying a vacuum to eliminate air bubbles. Then the elastomer was applied to both sides of the membrane support screen shown in Fig. 2. A spacer was placed on each side of the support and was compressed using an appropriate form at 1362 kg (3000 lb) of pressure.

The support and spacers were each 50-μm thick, resulting in a total membrane thickness of ~150 μm. The holes in the support were 0.556 cm in diameter. Preliminary observations using membranes without the supporting structure indicated that the membrane would not remain sufficiently rigid during the experiments. Since this would disturb the hydrodynamics at the surface and affect the diffusion layer thickness, a support was necessary. The membranes were measured with a micrometer at several places to obtain an average thickness.

Each membrane was allowed to cure for ~12 h. They were each removed and soaked in double-distilled water for ~15 min before use. The total area of membrane exposed to the solutions during the experiments was 6.16 cm^2, and the area of the holes through the support screen was 4.36 cm^2.

EXPERIMENTAL

Materials—Commercially available progesterone[5], radiolabeled progesterone[6], and radiolabeled capric acid[7] were used as received. The purity of the radioactive materials was checked periodically using TLC and were shown to be >98%. Polysorbate 80[8] and all other chemicals were used as received. Double-distilled water, degassed by boiling, was the only solvent used in preparing the permeant solutions.

Preparation of Solutions—All surfactant solutions were prepared by weighing polysorbate 80 into an appropriately sized volumetric flask and diluting with double-distilled water, previously degassed by bringing to a near boil, to obtain the correct percent weight/volume concentration of surfactant at 37°. This solution was allowed to equilibrate at 37° overnight before use. Saturated solutions were prepared by adding excess progesterone to surfactant solutions and equilibrating overnight. Before use, these solutions were filtered through two glass fiber filter papers[9] to eliminate particulates. Radioactive solutions were prepared by adding an aliquot of radiolabeled material to the test solution ~15 min before the experiment was begun.

Solubility Determination—The solubility of progesterone at several polysorbate 80 concentrations was determined by sealing ~5 ml of surfactant solution and excess progesterone in 15-ml ampuls and shaking in a 37° waterbath for 48 hr. Aliquots of equilibrated samples were filtered[9], diluted in ethanol USP, and assayed spectrophotometrically[10] at 240 nm. An identical solution, containing no progesterone and prepared in the same way, was used as a blank, and the absorbance was compared to a series of standards.

Viscosity and Density Determinations—The specific gravity of surfactant solutions was determined at 37° using a 25-ml pycnometer; the corresponding density, ρ, was calculated by calibrating the pycnometer with water (ρ = 0.993 g/cm^3 at 37°). Determinations of the kinematic viscosity, ν, were made with a viscometer[11]. The viscosity, η, was calculated from:

$$\nu = \eta/\rho \qquad \text{(Eq. 29)}$$

Diffusion Coefficient Determinations—Aqueous diffusion coefficients at 37° were determined using a small-volume diaphragm cell (14, 15). The apparatus consisted of two well-stirred reservoirs separated by two silver filter membranes[12]. Each membrane was 50-μm thick with a pore diameter of 1.2 μm. This pore diameter was large enough to permit the facile passage of micelles. The diffusion cell constant was determined using 0.1% benzoic acid in 0.01 *N* HCl for which the aqueous diffusion coefficient was known to be 1.4 × 10^{-5} cm^2/sec (16).

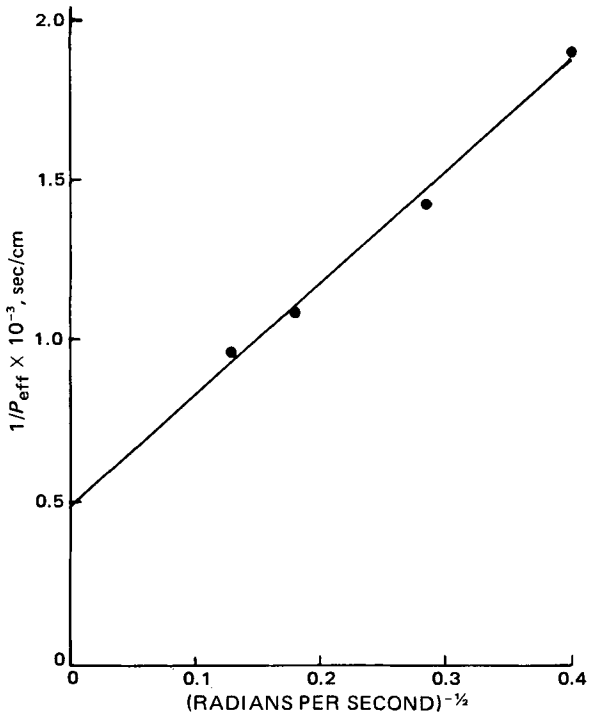

Figure 7—*Permeability coefficient dependence on rotation speed for progesterone.*

Subsequently, either the diffusion coefficient or the effective diffusion coefficient of progesterone in the presence of micelles was determined. Utilization of Eq. 9 permits the diffusion coefficient of the micelle to be factored out of the effective diffusion coefficient.

The effective diffusion coefficient was determined: (a) when only trace amounts of radiolabeled progesterone were present and (b) with surfactant solutions saturated with progesterone and containing sufficient radiolabeled progesterone to permit assay. In this way, any change in diffusivity with a change in progesterone concentration could be determined. All samples were assayed by adding the radioactive sample to 10 ml of liquid scintillation fluid[13] and counting in a liquid scintillation counter[14].

Diffusion Cell Characterization—To test the applicability of Eq. 20 to each side of the rotating membrane, radiolabeled capric acid was used. Since initial experiments showed this solute to have high membrane permeability, it was well suited for testing each diffusion layer separately by adjusting the pH in the donor and receiver solutions. For example, at sufficiently high pH in the receiver compartment, the diffusion of hydroxide ion from the bulk to the membrane surface essentially induces ionization of the permeant at the membrane surface. This results in "sink" conditions at the membrane surface being maintained with respect to the unionized species. If the membrane is impermeable to the ionized species, the receiver side diffusion layer resistance is eliminated or "shorted out." In this manner, the receiver side diffusion layer can be eliminated and the applicability of Eq. 20 to the donor side diffusion layer can be tested.

Prior to the start of each experiment, the prewashed membrane was positioned in the diffusion cell, which had been preheated in an oven to 37°. Then 70 ml of an appropriate solution (either 0.01 *N* HCl or 0.1 *M* phosphate buffer at pH 7.2) was added to the inner compartment. A visual inspection for leaks around the membrane was made. The diffusion cell was then immersed in an outer solution of 450 ml contained in a water-jacketed beaker to maintain the temperature of the outer solution and the diffusion cell at 37° for the duration of the experiment. The cell was rotated at 60, 120, or 300 rpm; 0.10-ml samples were withdrawn from both donor and receiver sides periodically. Assay for capric acid was by

[5] Aldrich Chemical Co., Milwaukee, Wis.
[6] Amersham Corp., Arlington Heights, Ill.
[7] California Bionuclear Corp., Sun Valley, Calif.
[8] Atlas Chemical Industries, Wilmington, Del.
[9] Whatman Filters, W&R Balston Ltd., England.
[10] Hitachi model 139, Hitachi Ltd., Tokyo, Japan.
[11] Size 25, Cannon-Fenske.
[12] Flowtronics, Philadelphia, Pa.
[13] ACS, Amersham Corp., Arlington Heights, Ill., and Aquasol, New England Nuclear, Boston, Mass.
[14] Model LS200, Beckman Instruments, Fullerton, Calif.

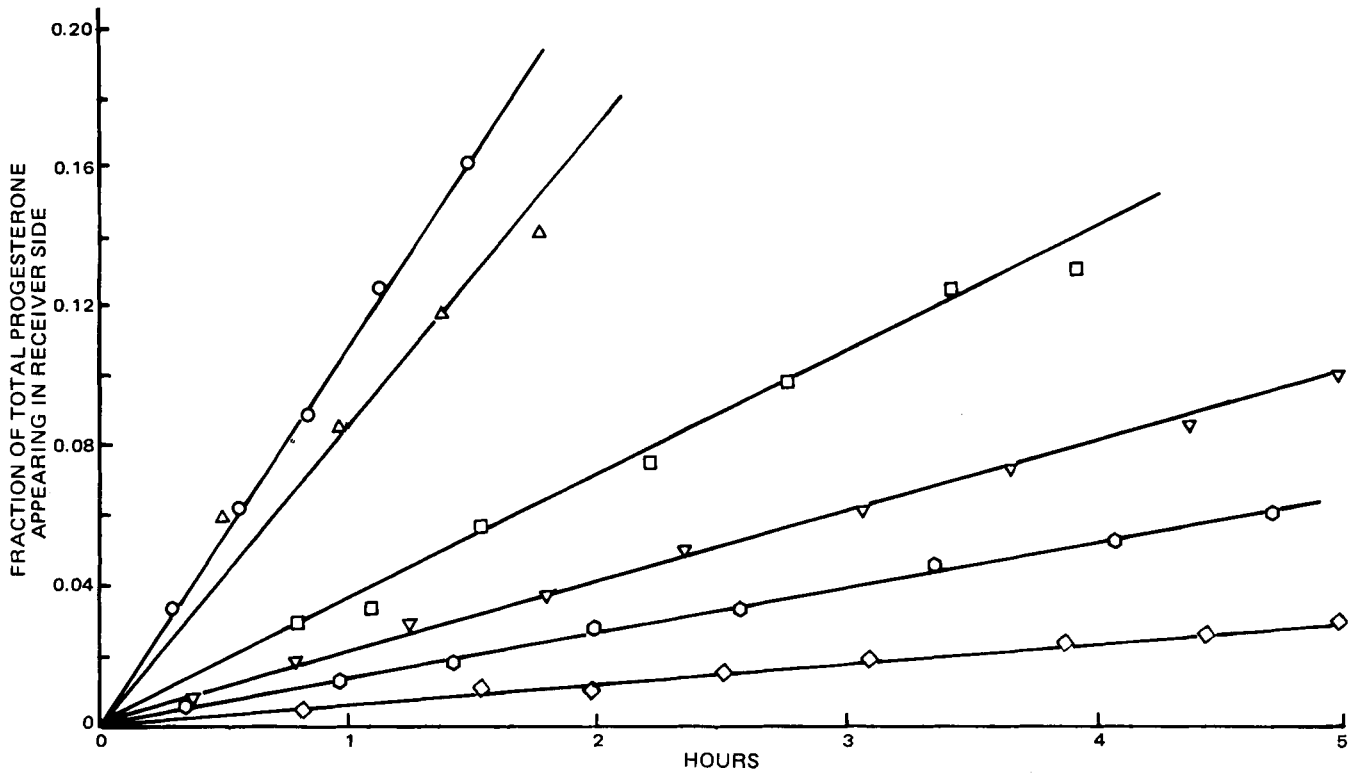

Figure 8—*Appearance of radiolabeled progesterone in the receiver compartment for constant initial concentration studies. Key (polysorbate 80 concentration):* ○, *0%;* △, *0.1%;* □, *0.5%;* ▽, *1.05%;* ○, *2.09%; and* ◇, *5.0%.*

liquid scintillation counting, and samples were corrected for quench if necessary. A series of steady-state experiments could be done in succession by completely replacing the receiver solution with fresh solution at the end of a run and, if necessary, replenishing the donor compartment with test permeant solution.

Micelle Solubilization Studies—The rotating-membrane diffusion cell was utilized for all transport experiments. The inner compartment served as the donor phase and the volume was 70 ml. The outer compartment volume was either 420 or 450 ml, depending on the experiment performed. Samples were taken using either a 100 or 500-μl Eppendorf micropipet[15]. Radioactive samples were assayed by liquid scintillation counting. Correction for quench was done when necessary. Nonradioactive progesterone was assayed by high-pressure liquid chromatography (HPLC) utilizing reversed-phase chromatography[16].

Two types of experiments were conducted to demonstrate clearly the influence of progesterone concentration on transport in the presence of polysorbate 80. Constant initial solute concentration experiments were carried out by adding an aliquot of radiolabeled progesterone (approximately the same concentration for each experiment) to 70 ml of surfactant solution, and saturated solution experiments were performed by adding surfactant solutions previously saturated with nonradiolabeled progesterone to the donor compartment. An identical surfactant solution with no progesterone was used as the receiver phase in each case.

In all experiments, samples were taken from the donor and receiver phases and assayed by liquid scintillation counting or HPLC. All experiments were conducted at 37° and a rotation speed of 60 rpm.

RESULTS AND DISCUSSION

The aqueous solubility of progesterone at 37° was determined to be 12.0 μg/ml, and the total solubility of progesterone increased linearly with increasing surfactant concentration over the range studied. The slope of the line is related to the micelle-free solute equilibrium distribution coefficient, k^*, by:

$$C_T = C^* + C' = C'[1 + k^*(SAA)] \qquad \text{(Eq. 30)}$$

The slope of the line was 1.26×10^{-1} mg/ml percent and corresponded to a value of 10.5 for the equilibrium distribution coefficient. This result is consistent with independent but less reliable measurements conducted in this laboratory using dialysis tubing.

The kinematic viscosity is shown in Fig. 3. The density increased linearly with surfactant concentration from a value of 0.993 g/cm^3 for pure water at 37° to 1.002 g/cm^3 for an 8.5% (w/v) polysorbate 80 solution.

The effective diffusion coefficients at several surfactant concentrations, as determined by using the small-volume diaphragm cell, are presented in Table I. The effective diffusion coefficient decreased as the surfactant concentration increased due to incorporation of more solute into the micelles. The effective diffusion coefficient was determined for both tracer levels of progesterone and saturated solutions. As shown, there was little difference between the diffusion coefficients at comparable surfactant concentrations and it is concluded that D_{eff} does not vary significantly with progesterone concentration.

By utilizing Eq. 9*a*, the diffusion coefficient of the micelle–solute complex (D^*) can be evaluated if the micelle-free solute equilibrium coefficient (k^*) and the free solute diffusion coefficient (D') are known. These values are shown in Table I, assuming a free solute diffusivity of 8.5×10^{-6} cm^2/sec and a micelle-free solute equilibrium coefficient of 10.5. For the progesterone–polysorbate 80 system under investigation, D^* is not constant.

Diffusion Cell Characterization—Typical results of the rate of loss of radiolabeled capric acid from the donor phase for three rotation speeds are shown in Fig. 4 when both the donor and receiver phases are 0.01 *N* HCl solutions. The diffusion layers on each side of the semipermeable membrane, thus, are important barriers to transport. The rate of loss of capric acid from the donor phase, for the same three rotation speeds, with 0.1 *M* phosphate buffer at pH 7.2 as the receiver side solution is shown in Fig. 5. The donor side diffusion layer is the only diffusion layer offering resistance to diffusion in this second case.

The effective permeability of the diffusional resistance under quasi-steady-state conditions can be conveniently assessed from the slope of the semilogarithmic plots by:

$$\ln (C_t/C_0) = \frac{-A}{V} P_{eff} t \qquad \text{(Eq. 31)}$$

where C_t is the concentration of solute remaining in the donor phase at time t, C_0 is the initial concentration, V is the volume of the donor phase, and A the area of the membrane available for transport. The area in these studies is the area of the holes in the membrane support (4.36 cm^2). Equation 31 can be modified to correct for any buildup of solute in the receiver compartment when necessary.

[15] Brinkmann Instruments, Westbury, N.Y.

[16] Model 440 equipped with μBondapack C_{18} column, Waters Associates, Milford, Mass.

Table III—Theoretical and Experimental Slopes of $1/P_{eff}$ *versus* $\omega^{-1/2}$ Plots

pH			Theoretical	Experimental	*SD*
Inner	Outer	*n*	Slope × 10^{-3}	Slope × 10^{-3}	× 10^{-3}
2.0[a]	2.0	5	3.672	3.56	0.44
2.0[a]	7.2	5	1.836	1.87	0.30
7.2	2.0[a]	3	1.836	1.62	0.18

[a] Denotes donor compartment.

The reproducibility of the effective permeability coefficient determinations utilizing the rotating-membrane diffusion cell is shown in Table II. Duplicate experiments in which both donor and receiver compartments were prepared from 0.01 *N* HCl solutions were performed. The average permeability and the standard deviation determmined at 60, 120, and 300 rpm are given. The coefficient of variation for each speed was between 5 and 6%. These deviations include sampling and assay errors as well as some variations in membrane thickness. Each experiment was done with a new membrane. Generally, the observed reproducibility compares with that observed for published work with other diffusion cell systems, indicating satisfactory reproducibility for each experiment.

The applicability of Eq. 20 to the diffusion layer thickness on each side of the membrane can be tested by utilizing Eqs. 27 and 28. Figure 6 depicts the results obtained when the inverse of the permeability is plotted against the inverse square root of the rotation speed for three different conditions. Both the donor and receiver side diffusion layers are important in Fig. 6A, and Eq. 27 should apply. The theoretical slope is 3.672 × 10^3, assuming a diffusion coefficient for capric acid (17) of 7.5 × 10^{-6} cm^2/sec and a kinematic viscosity of 6.96 × 10^{-3} cm^2/sec. Figures 6B and 6C show the results obtained when the outer and inner diffusion layer resistance are eliminated by buffering at pH 7.2. Consequently, Eq. 28 should apply. The theoretical slope is half of that for Eq. 27 or 1.836 × 10^3. The intercept corresponding to the inverse of the membrane permeability should be the same in each case.

Table III presents results from duplicate experiments like those given in Fig. 6. The average slope of 3.56 × 10^3 agrees quite closely with the theoretical prediction of 3.672 × 10^3 when both diffusion layers are included. When the outer or inner diffusion layer is eliminated, the average of the experimentally determined slope is 1.87 or 1.62 × 10^3, respectively. The Student *t* test for significance of difference between two means at the 5% level of confidence indicates there is no statistical difference between the latter two slopes. The 11–16% coefficient of variation for each case can be attributed in part to the 5–6% variation observed in each determination.

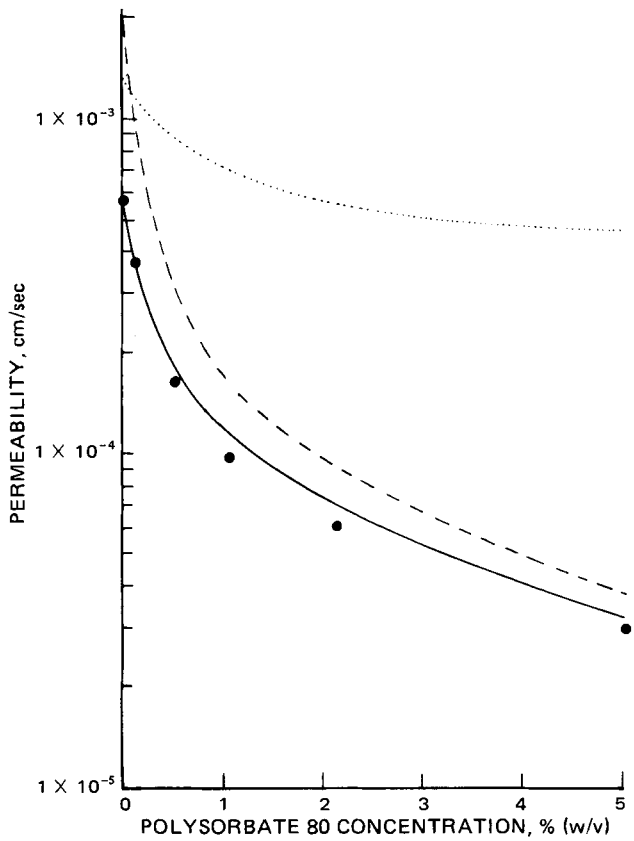

Figure 9—*Theoretical predictions of* P_{eff} (—), P_m (- - -), *and* P_i (· · ·) *as a function of polysorbate 80 concentration based on independent estimates of the physicochemical parameters. Key:* ●, *experimentally determined* P_{eff}.

Table IV—Experimentally Determined Permeability Coefficients and Fluxes from Constant Initial Concentration and Saturated Solution Studies

Polysorbate 80 Concentration, %	Constant Initial Concentration Case, P_{eff} × 10^4, cm/sec	Saturated Solution Case	
		Flux from Saturated Solution × 10^9, g/cm^2 sec	P_{eff} × 10^4, cm/sec
0	5.87	7.05	5.87
0.1	3.75	—	—
0.126	—	9.42	2.89
0.5	1.65	—	—
0.52	—	14.65	1.78
1.05	0.965	—	—
2.04	—	16.98	0.62
2.09	0.612	—	—
5.0	0.30	—	—

Because of the close agreement between theory and experiment, these results indicate that the aqueous diffusion layer thickness on each side of the rotating membrane is equal within the limits of experimental error. Therefore, Eq. 20 applies for each diffusion layer thickness. This diffusion cell system also has the advantage of permitting easy and quantitative control of the aqueous diffusion layer thickness and gives more insight into the events occurring within it. The ability to extrapolate to infinite rotation speed also permits the diffusion layer resistance to be factored out, thereby permitting an estimate of the membrane permeability coefficient.

Equation 27 can be utilized to determine the membrane permeability coefficient and the aqueous diffusion coefficient of progesterone, and results are presented in Fig. 7. The membrane permeability coefficient is estimated from the intercept to be 2.0 × 10^{-3} cm/sec for a 190-μm thick membrane. The aqueous diffusion coefficient, estimated from the slope in Fig. 7, is 8.5 × 10^{-6} cm^2/sec. This value is close to the diffusion coefficient of 7.9 × 10^{-6} cm^2/sec as determined by the small-volume diaphram cell method.

Micelle Solubilization Studies—The appearance of radiolabeled progesterone in the receiver compartment is shown in Fig. 8 for several polysorbate 80 concentrations. In these studies, the donor compartment contained approximately equivalent initial concentrations of radiolabeled progesterone. A decreasing slope as the surfactant concentration is increased is seen, reflecting a decreasing permeability. The effective permeability coefficients as determined from the slope of the lines in Fig. 8 are given in Table IV and are included in Fig. 9 along with theoretical estimates from the model. The theoretical estimates were based on Eqs. 24 and 25 and independent estimates of all relevant physicochemical parameters.

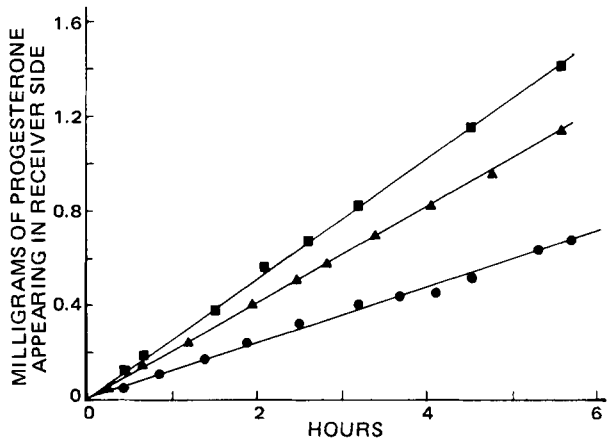

Figure 10—*Appearance of progesterone in the receiver compartment from saturated solutions. Key: (polysorbate 80 concentration)* ■, *2.04%;* ▲, *0.52%; and* ●, *0.126%.*

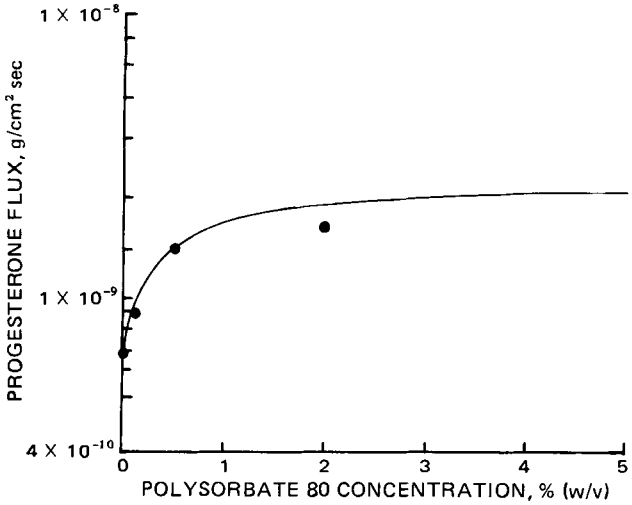

Figure 11—*Flux of progesterone from saturated solutions as a function of polysorbate 80 concentration. Key: —, theory; and ●, experimental.*

There is very good agreement between experimental results and the theoretical model. The predicted change in the permeability coefficient of the aqueous diffusion layer resistance is also included (P_i). It approaches a limiting value at high surfactant concentrations, corresponding to the permeability coefficient of the diffusion layer when only micelles are transported. The effective permeability coefficient continues to decrease, however, since the thermodynamic activity of progesterone continues to decrease with increasing surfactant. The theoretical curve labeled P_m is obtained when the aqueous diffusion layer is completely neglected.

The decreasing flux as a function of surfactant concentration is a result of the decreasing aqueous permeability coefficient and also the decreasing thermodynamic activity of progesterone. The decreasing effective permeability coefficient is in part the result of the changing aqueous diffusion layer permeability coefficient given in Eqs. 8 and 25. As the surfactant concentration increases, more progesterone is incorporated within the micelle and most of the progesterone diffuses through the diffusion layer solubilized in the micelle. The smaller diffusivity of the micelle determines the aqueous permeability coefficient at high surfactant concentrations. The thermodynamic activity of progesterone is also affected by the surfactant concentration since the concentration of free progesterone in the aqueous phase is lower due to micelle solubilization. This situation is reflected in the membrane permeability, P_m, and also in the bulk aqueous phase through Eq. 4.

Saturated Solution Studies—The rate of appearance of progesterone in the receiver side is shown in Fig. 10 for three surfactant concentrations. The donor phase was presaturated with progesterone, and the appearance of solute in the reciever side was followed using HPLC. The corresponding fluxes of progesterone from each of these saturated solutions is shown in Fig. 11, and the corresponding effective permeability coefficients are tabulated in Table IV. The solid line in Fig. 11 is the theoretical prediction based upon Eqs. 23 and 24 and is included to show the close agreement between experimental results and theoretical predictions based on the physical model and independent estimates of the relevant physicochemical parameters.

As was the case for the constant initial progesterone concentration studies, the effective permeability coefficient for the trilaminar resistance decreases with increasing surfactant concentration. However, a larger total bulk solute concentration, C_{b1}, is possible due to micelle solubilization. For the progesterone–polysorbate 80 case, the increased solubility of progesterone offsets the decreased permeability; the net result is an increase in flux as the surfactant concentration increases. In effect, the micelles act as carriers of solute across the aqueous diffusion layer to the membrane surface. In this way, the diffusion layer resistance can be eliminated or shorted out. At high surfactant concentrations, saturated solution conditions can be reached at the membrane surface and the membrane is the only resistance to diffusion. For progesterone, this plateau occurs at ~2% polysorbate 80 and there is little further increase in flux.

REFERENCES

(1) G. Levy and R. H. Reuning, *J. Pharm. Sci.*, **53**, 1471 (1964).

(2) C. L. Gantt, N. Gachman, and J. M. Dyniewics, *Lancet*, **1**, 486 (1961).

(3) C. H. Jones, P. J. Culver, G. D. Drummey, and A. E. Ryan, *Ann. Intern. Med.*, **29**, 1 (1948).

(4) J. G. Wagner, E. S. Gerard, and D. G. Kaiser, *Clin. Pharmacol. Ther.*, **7**, 610 (1966).

(5) G. Levy and J. A. Anello, *J. Pharm. Sci.*, **57**, 101 (1968).

(6) G. B. Dermer, *J. Ultrastructure Res.*, **20**, 311 (1967).

(7) H. Westergaard and J. M. Dietschy, *J. Clin. Invest.*, **58**, 97 (1976).

(8) N. E. Hoffman and W. J. Simmonds, *Biochim. Biophys. Acta*, **241**, 331 (1971).

(9) T. Karman, *Z. Angew. Math. Mech.*, **1**, 244 (1921).

(10) W. J. Albery, J. F. Burke, E. B. Leffler, and J. Hadgraft, *J. Chem. Soc. Faraday Trans.*, **1**, **72**, 1618 (1976).

(11) E. G. Lovering and D. B. Black, *J. Pharm. Sci.*, **63**, 671 (1974).

(12) E. R. Garrett and P. B. Chemburkar, *ibid.*, **57**, 944 (1968).

(13) V. G. Levich, "Physicochemical Hydrodynamics," Prentice-Hall, Englewood Cliffs, N.J., 1962.

(14) M. M. Kreevoy and E. M. Wewerka, *J. Phys. Chem.*, **71**, 4150 (1967).

(15) K. H. Keller, E. R. Canales, and S. S. Yun, *ibid.*, **75**, 379 (1971).

(16) S. Prakongpan, Ph.D. thesis, University of Michigan, Ann Arbor, Mich., 1974.

(17) D. E. Bidstrup and C. J. Geankoplis, *J. Chem. Eng. Data*, **8**, 170 (1963).